Fast CMOS-Integrated Finger Photodiodes for a Wide Spectral Range

H. Zimmermann, H. Dietrich
Institut für Elektrische Mess- und Schaltungstechnik, Technische Universität Wien,
Gusshausstrasse 25/354, A-1040 Wien, Austria
horst.zimmermann@ieee.org

A. Ghazi, P. Seegebrecht
Lehrstuhl für Halbleitertechnik,
Christian-Albrechts-Universität
Kaiserstrasse 2, D-24 143 Kiel, Germany
ps@tf.uni-kiel.de

Abstract

A new monolithically integrated photodiode in CMOS technology using p-type substrate is presented. This photodiode is optimized for a high speed and a wide spectral range from red to blue/UV. The cathode finger structure of the photodiode increases the quantum efficiency for a wavelength of 400 nm to 46 % compared to a value of 14 % for a conventional photodiode without a finger cathode. With an antireflection coating a further increase to a quantum efficiency of 70 % is possible for the finger photodiode. Rise and fall times below 1 ns are measured for this photodiode for red and UV light. The corresponding bandwidths are larger than 470 MHz. Such a fast and highly efficient photodiode is needed in near-future optoelectronic integrated circuits (OEICs) for applications in optical storage systems like DVD (Digital Versatile Disk) and DVR (Digital Video Recording).

1. Introduction

The market for optical storage systems is rapidly growing. While todays CD-ROMs using a laser diode with a wavelength of 780 nm have a capacity of 650 MB, future DVD-ROMs will use a wavelength of 400 nm to achieve a storage capacity of more than 30 GB. This is accomplished not only by the use of multilayer disks but also by the use of smaller dimensions on the disk itself, for which the availability of UV/blue semiconductor laser diodes [1] with a sufficient lifetime is a prerequisite. In todays DVD optical pickups, red laser diodes with a wavelength of 650 nm are used. Intensive research and development is being done by many companies to make blue DVR available to the customer. In turn, read-out sensors (OEICs), which are fast and sensitive for both UV/blue and red laser light, for compatibility reasons, are soon necessary.

The 1/e-absorption depth of light with a wavelength of 400 nm in silicon is less than 0.1 μm. Considering a conventional pn-photodiode with a non-interdigitated n^+-surface cathode we can conclude that almost all of the incident photons are absorbed in the quasi neutral region of the n^+-cathode, which normally has a depth of 0.2 - 0.4 μm. The majority of the photogenerated carriers, therefore, will recombine in the n^+-cathode, because of slow carrier diffusion due to the low electron and hole mobilities (keeping the Einstein relation in mind) in the highly doped cathode. As a consequence of this strong recombination, the responsivity and the quantum efficiency for $\lambda = 400$ nm with a non-interdigitated cathode is low. Furthermore, the slow carrier diffusion processes outside the space-charge region are responsible for a limited response speed.

For 400 nm, a lateral SOI photodiode suggested in [2] would be a good choice. An SOI photodiode, however, shows a low quantum efficiency for red light due to the 1/e-penetration depth of about 2.8 μm for red light and due to the thin SOI layer. Bulk silicon photodiodes, therefore, have to be preferred when a high quantum efficiency is required in a wide spectral range from the red/infrared to UV. Several attempts towards bulk silicon high-efficiency-UV photodiodes were reported. In [3], for instance, a quantum efficiency of 53% was reported for λ = 400 nm for a photodiode inside the n-well. A p-i-n junction-surface depletion-layer photodiode with a quantum efficiency of about 56% for λ = 400 nm was investigated in (111)-oriented silicon [4]. No transient results, however, were shown in [3, 4]. Avalanche photodiodes (APDs) were investigated to enhance the sensitivity further. In [5] a responsivity of about 2.3 A/W at 400 nm was achieved for a reverse bias of 19.1 V with an APD consisting of p^+-source/drain and an interrupted n-well in CMOS technology. In [6], a UV-selective APD was presented, which achieved a responsivity of 5.3 A/W at 380 nm with a reverse bias of 14.5 V. The high voltages required for APD photodiodes, however, are not available in modern optical storage systems. Furthermore, the sensitivity of APDs for longer wavelengths is much lower than for 400 nm.

2. Structure of the finger photodiode

The finger photodiode in bulk CMOS technology allows a high quantum efficiency in a wide spectral range. To avoid both, recombination and diffusion, space-charge regions at the surface have to be implemented. We propose an interdigitated structure as it is shown in Fig. 1. The p^+-substrate is used as the anode and the n^+-fingers, which are located in the p-epitaxial layer, are used as the cathode of the photodiode. The n^+-fingers are connected by metal outside of the photo-sensitive region. Photogen-

erated carriers can be separated in the space-charge region, electrons drift to the n^+-fingers and holes drift to the p^+-substrate.

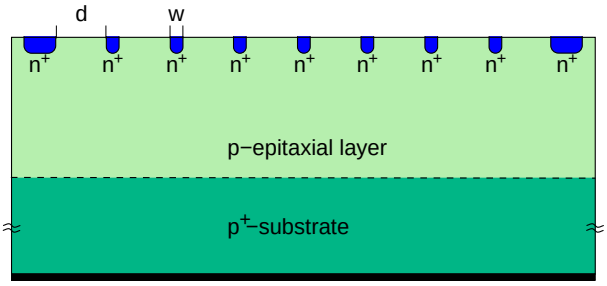

Figure 1. Cross section of 9-finger photodiode on p-substrate

Due to the improvement of the rise and fall times of pin-photodiodes on n-type substrate with a reduced doping concentration C_e in the epitaxial layer [7], we varied this doping concentration. In order to find the optimum concerning response speed and quantum efficiency, we have processed several finger photodiodes with different numbers of fingers. We used an industrial 1 μm twin-well CMOS process (not implementing a self-adjusting well process scheme) with one additional mask to block out the threshold voltage implantation between the n^+-fingers in the photo-active region. No antireflection coating (ARC) was implemented in the photo-active region.

3. Measurement set-up

For measurements, integrated polysilicon resistors with a resistance of $R_L = 0.5\,\mathrm{k\Omega}$ for $\lambda = 638\,\mathrm{nm}$ and $R_L = 1\,\mathrm{k\Omega}$ for $\lambda = 400\,\mathrm{nm}$ (because of different optical signal power) are connected in series with the photodiodes. The laser light is coupled into the photodiode (photo-active area: $50 \times 50\,\mu\mathrm{m}^2$) via an optical fiber resulting in a light-spot diameter of less than 40 μm on the integrated photodiodes. The photocurrent results in a voltage across R_L, which is measured with a picoprobe (with an input capacitance of 0.1 pF, a bandwidth of 3 GHz, and an attenuation of 20). For the transient measurements a sampling oscilloscope (HP 54750A) was used. The dark currents were measured with a semiconductor parameter analyzer (HP 4156A). A calibrated photodiode was used to determine the incident optical power for quantum efficiency measurements at the finger photodiodes.

4. Results

A responsivity of 0.148 A/W at 400 nm ($\eta = 0.46$) was measured for the 9-finger photodiode compared to 0.045 A/W ($\eta = 0.139$) for a reference photodiode having a non-interdigitated cathode both without antireflection coating (ARC). For $\lambda = 638\,\mathrm{nm}$ the 9-finger photodiode has a responsivity of 0.30 A/W ($\eta = 0.55$) without ARC independent of C_e. Optical simulations showed that a quantum efficiency of 70 % for 400 nm and of 95 % for 638 nm is achievable with a SiO_2-Si_3N_4 antireflection coating. A quantum efficiency of 94 % was verified for 638 nm experimentally with such an antireflection coating for a nip-photodiode on p-substrate with a non-interdigitated cathode integrated in the same CMOS process [8].

In order to find the optimized interdigitated structure for a high quantum efficiency and short rise and fall times we processed the finger photodiodes with different numbers of fingers for a constant area of the photodiodes. The distance d between the fingers and the finger width w (see Fig. 1) were varied, because the rise and fall times cannot be predicted reliably enough by analytical calculations due to a two-dimensional electric-field distribution. In addition a contribution of carrier diffusion makes a prediction even more difficult. Table 1 summarizes the measured results for the 3-, 4-, 6-, and 9-finger photodiodes ($\lambda = 400\,\mathrm{nm}$) with a reverse bias of $V_{PD} = 3\,\mathrm{V}$.

Table 1. Rise and fall times of finger photodiodes on p-type substrate with different numbers of fingers ($C_e = 1 \times 10^{15}\,\mathrm{cm}^{-3}$, $\lambda = 400\,\mathrm{nm}$, $R_L = 1\,\mathrm{k\Omega}$, $V_{PD} = 3\,\mathrm{V}$)

Fingers	d [μm]	w [μm]	t_r [ns]	t_f [ns]
3	18.6	4.2	1.60	1.74
4	12.8	2.8	1.56	1.56
6	8.0	1.6	1.22	1.22
9	4.8	1.2	0.65	0.83

The fastest finger photodiode is the one with 9 fingers. The space-charge regions of neighboring n^+ regions overlap and there is no carrier diffusion involved. Drift of photogenerated carriers leads to the fast response for the 9-finger photodiode with $C_e = 1 \times 10^{15}\,\mathrm{cm}^{-3}$. For the 3-, 4- and 6-finger photodiodes the distance of the cathode fingers is so wide that carrier diffusion should be expected to contribute and to slow down the response speed. The rise and fall times of 1.60 ns and 1.74 ns for the 3-finger photodiode, however, are rather short for a d of 18.6 μm. The short rise and fall times of the 3-, 4-, and 6-finger photodiodes, therefore, have to be explained like this: due to positive oxide and Si-SiO_2-interface charges, there is an n-type inversion layer between the n^+ fingers leading to an nip-photodiode actually rather than a finger photodiode. The electric field in such a nip photodiode is vertical without lateral components between the two cathode space-charge regions (SCRs, see Fig. 2). Therefore, the drift time is about the same for the 3-, 4-, and 6-finger photodiodes. For the 3-finger photodiode the series resistance in the inversion layer is largest. Therefore, the rise and fall times of this photodiode are the longest due to an RC-time constant (together with the capacitance of the photodiode).

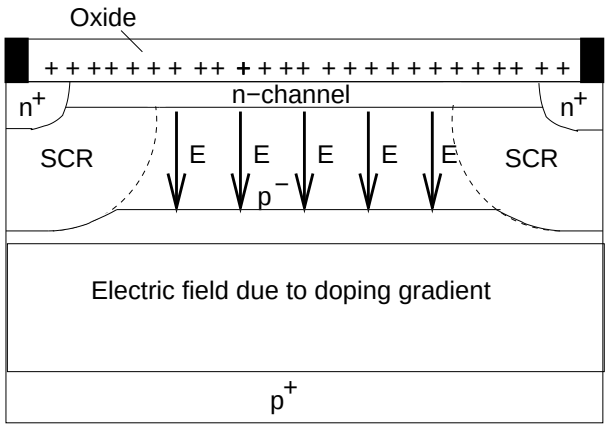

Figure 2. Electric field in a finger photodiode with C_e=1 × 10^{15} cm^{-3} due to positive oxide charges and due to boron out-diffusion from the p^+ substrate

The vertical electric field due to positive oxide charges and the series resistance in the inversion layer explain the rather similar rise and fall times of the 3-, 4-, and 6-finger photodiodes. Nevertheless, the most important factor for a fast response is d. It has to be small enough to eliminate the series resistance in the inversion layer. The n^+ width w also determines the series resistance of the cathode, which is of minor importance. A small w, i. e. a large ratio of d/w is necessary for a high quantum efficiency in the blue/UV spectral range.

Table 2. Rise and fall times of the 9-finger photodiode on p-type wafers with different epitaxial doping concentrations ($R_L = 0.5\,k\Omega$ for $\lambda = 638\,nm$, $R_L = 1\,k\Omega$ for $\lambda = 400\,nm$, $V_{PD} = 3\,V$).

	638 nm		400 nm	
C_e [cm^{-3}]	t_r [ns]	t_f [ns]	t_r [ns]	t_f [ns]
5×10^{13}	0.31	0.82	0.90	1.0
1×10^{14}	0.32	0.88	0.69	0.87
1×10^{15}	0.36	1.02	0.65	0.83

Table 2 lists the measured rise and fall times for 9-finger photodiodes with different epitaxial doping concentrations. The values for red light were corrected for the laser and picoprobe rise and fall times. For red light and $C_e = 1 \times 10^{15}\,cm^{-3}$, the rise and fall times of the 9-finger photodiode are 0.36 and 1.02 ns, respectively, which are very low values for this standard doping concentration in the epitaxial layer. The space-charge region extends only about 2 μm at the reverse bias of 3 V, whereas carriers are generated to a depth of about 10 μm (in a depth of 4 times the 1/e-penetration depth the optical power decreases to the one percent region) by light with a wavelength of 638 nm. Carrier diffusion, however, is obviously almost unimportant. This unexpected effect can be explained by a rather thin epitaxial layer and by out-diffusion of the p^+-substrate leading to a doping gradient and an associated electric field within the penetration depth of red light (see Fig. 2). Therefore, almost no carrier diffusion slows down the rise and fall times.

When the doping concentration is reduced to $C_e = 1 \times 10^{14}\,cm^{-3}$ and below, the space-charge region widens from the pn-junction and the rise and fall times for 638 nm decrease. The strong asymmetry between rise and fall times is due to a strong overshoot of the optical power emitted by the red laser diode used for characterization of the photodiodes. When the light is switched off, there is no undershoot, however [9]. Therefore, the fall time is not shortened in contrast to the rise time. The asymmetry in the rise and fall times of the measured photocurrent is caused by the laser overshoot, which also leads to an asymmetry of the laser rise and fall times of course.

Figure 3 shows the transient response of the 9-finger photodiode for a wavelength of 638 nm and for C_e=5 × 10^{13} cm^{-3}. The overshoot of the optical power emitted by the laser diode is almost suppressed due to the rising edge of the photocurrent transient in the finger photodiode, which has almost the same duration as the overshoot.

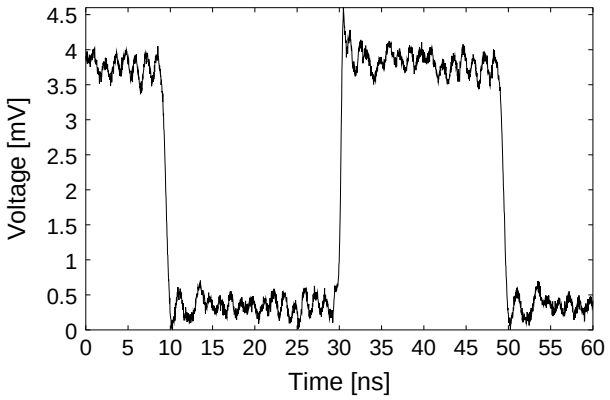

Figure 3. Transient response of the 9-finger photodiode (C_e=5 × 10^{13} cm^{-3}, $\lambda = 638\,nm$, $R_L = 0.5\,k\Omega$, $V_{PD} = 3\,V$)

For UV light, the rise times listed in Tab. 2 seem longer than that for red light because no correction for the laser rise and fall times could be made due to missing blue-laser data. They, however, are shortest for $C_e = 1 \times 10^{15}\,cm^{-3}$ (see Tab. 2). For this doping concentration the space-charge region for a reverse bias of 3 V is already larger than the 4/e-penetration depth of light with a wavelength of 400 nm. The rise and fall times slightly increase when the doping concentration in the epitaxial layer is reduced (see Tab. 2). This can be explained by an increase of the thickness of the space-charge region with a reduced doping concentration in the epitaxial layer. A thicker space-charge region leads to a longer drift time and therefore to longer rise and fall times. Fig. 4 shows the transient response of the 9-finger photodiode for a wavelength of 400 nm.

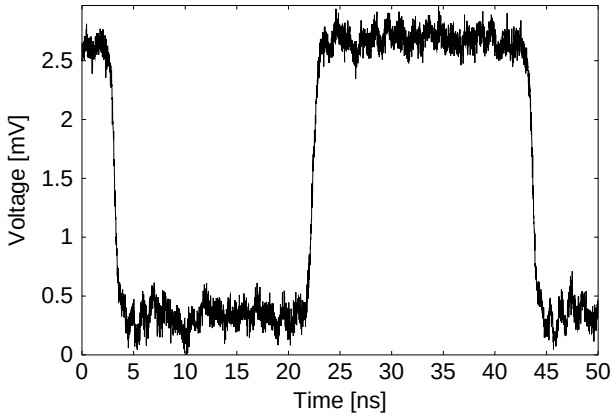

Figure 4. Transient response of the 9-finger photodiode (C_e=5×10^{13} cm^{-3}, $\lambda = 400$ nm, $R_L = 1$ kΩ, $V_{PD} = 3$ V)

The bandwidth of photodiodes can be estimated according to $f_{3dB} = 2.2/(\pi(t_r + t_f))$. For the 9-finger photodiode and C_e=1×10^{15} cm^{-3} we obtain a bandwidth of 470 MHz for 400 nm and 510 MHz for 638 nm.

In OEICs for optical storage systems a low offset voltage is required [10]. Therefore the dark current of the photodiode which is connected to the input of the amplifier has to be small. Fig. 5 shows the measured dark currents of the 9-finger photodiode for different temperatures. The dark current is below 10 pA for temperatures up to 75 °C. Even for reverse voltages above 3 V the dark current remains significantly small.

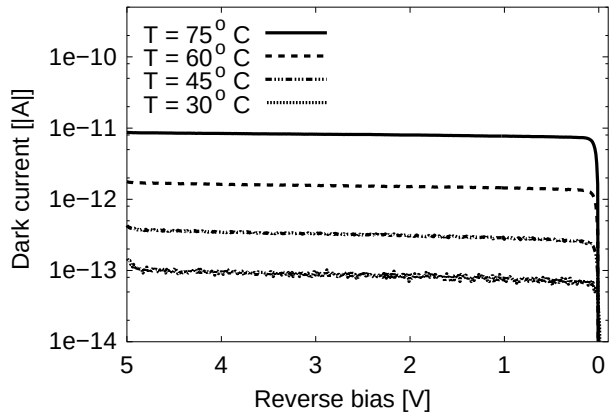

Figure 5. Dark current of the 9-finger photodiode on a wafer with $C_e = 5 \times 10^{13}$ cm^{-3} for different temperatures

5. Conclusions

With the innovative finger photodiodes the responsivity for $\lambda = 400$ nm is increased by a factor of 3.3 compared to a conventional photodiode and rise and fall times of less than 0.9 ns are obtained for the standard epi concentration. The finger photodiodes have a responsivity of 0.30 A/W for $\lambda = 638$ nm and rise and fall times of less than 1.0 ns for $C_e \leq 1 \times 10^{15}$ cm^{-3}. A reduction of the doping concentration in the epitaxial layer below the standard doping concentration of 1×10^{15} cm^{-3} is not necessary to achieve bandwidths of 470 MHz and 510 MHz for 400 nm and 638 nm, respectively. The dark currents of the finger photodiodes are below 10 pA even at a temperature of 75 °C. The finger photodiodes can be integrated in twin-well CMOS-processes with little modifications and are therefore well suited for UV/blue-sensitive OEICs for optical storage systems of the next generation, which are compatible with todays optical storage systems using red light.

6. Acknowledgements

The authors would like to thank Mrs. R. Popp and Mr. R. Buchner for the fabrication of the photodiodes at the Fraunhofer Institute for Solid-State Technology in Munich, Germany. Furthermore we would like to thank M. Wieseke for some measurements and T. Heide as well as M. Hohenbild for valuable discussions. Parts of this project were funded by the German 'Bundesministerium für Bildung, Wissenschaft, Forschung und Technologie' (BMBF) under reference 01BS604/5.

[1] S. Nakamura and G. Fasol, *The Blue Laser Diode*, Springer, Heidelberg, 1998.

[2] J.-P. Colinge, "p-i-n photodiodes made in laser-recrystallized silicon-on-insulator," *IEEE Trans. on Electron Devices*, vol. 33, February 1986, pp. 203-205.

[3] A. Pauchard, P.-A. Besse, and R. S. Popovic, "A Silicon Blue/UV Selective Stripe-Shaped Photodiode", *Sensors and Actuators*, vol. 76, 1999, pp. 172-177.

[4] C. S. Yin, "The p-i-n Junction-Surface Depletion-Layer Photodiode", *IEEE Electron Device Letters*, vol. 12, August 1991, pp. 442-443.

[5] A. Pauchard, A. Rochas, Z. Randjelovic, P.-A. Besse, and R. S. Popovic, "Ultraviolet Avalanche Photodiode in CMOS Technology", *Technical Digest Int. Electron Dev. Meeting 2000*, pp. 709-712.

[6] A. Pauchard, P.-A. Besse, and R. S. Popovic, "Dead Space Effect on the Wavelength Dependence of Gain and Noise in Avalanche Photodiodes", *IEEE Trans. on Electron Devices*, vol. 47, September 2000, pp. 1685-1693.

[7] H. Zimmermann, *Integrated Silicon Optoelectronics*, Springer, Berlin, Heidelberg, 2000, pp. 61-65.

[8] H. Zimmermann, K. Kieschnick, T. Heide, A. Ghazi, "Integrated High-Speed High-Responsivity Photodiodes in CMOS and BiCMOS Technologies", *Proc. 29th European Solid-State Device Research Conference (ESSDERC)*, Edition Frontieres, 1999, pp. 332-335.

[9] K. J. Ebeling, *Integrated Optoelectronics*, Springer, Berlin, Heidelberg, 1993.

[10] A. Ghazi, T. Heide, H. Zimmermann, P. Seegebrecht, "DVD OEIC and 1 GBit/s Fiber Receiver in CMOS Technology," *Proc. 7th IEEE Int. Symposium on Electron Devices for Microwave and Optoelectronic Applications (EDMO) 2000*, Glasgow, UK, pp. 224-229.